Flow, Turbulence and Combustion
https://doi.org/10.1007/s10494-024-00578-8

RESEARCH

Experimental and Full-Annulus Simulation Analysis of the Rotating Stall in a Centrifugal Compressor Stage with a Vaned Diffuser

Yufang Zhang[1] · **Shuai Li**[2] · **Hechun Yu**[2] · **Linlin Cui**[2]

Received: 29 November 2023 / Accepted: 3 August 2024

Abstract
Flow instability such as rotating stall and even surge occurs when the centrifugal compressor stage operates under low flow conditions. This phenomenon is an extremely complex dynamic process, and it is closely related to the aerodynamic performance and internal flow of the stage. Therefore, it is necessary to study the flow development characteristics in the stage. This paper employs experimental measurement and full-annulus numerical simulation to investigate the effects of diffuser stall on the aerodynamic performance of the compressor and the internal flow of the impeller. The propagation direction, speed, evolution characteristics, and the number of the stall cell were obtained by experimental measurement, and the numerical simulation method was verified. The numerical results that there is a stall limit cycle with counter-clockwise rotation between the flow rate and total pressure ratio of the compressor when the diffuser stalls. Meanwhile, it is found that the stall limit cycle is closely related to the separation strength of the internal flow in the compressor. Finally, the coherent flow structure near the vane shroud side is identified by the modal decomposition methods when the diffuser stalls. The research results in this paper promote an in-depth understanding of the stall mechanism of centrifugal compressors.

Keywords Centrifugal compressor stage · Vaned diffuser · Rotating stall · Stall limit cycle · Modal decomposition

List of symbols

POD	Proper Orthogonal Decomposition
DMD	Dynamic Mode Decomposition
IGV	Inlet guide vane
BPF	Blade passing frequency
D_2	Impeller outlet diameter
D_3	Diffuser inlet diameter

✉ Shuai Li
lishuai23@zut.edu.cn

[1] College of Mechanical and Electrical Engineering, Zhengzhou Railway Vocational and Technical College, Zhengzhou 451460, China

[2] School of Mechatronics Engineering, Zhongyuan University of Technology, Zhengzhou 450007, China

Published online: 07 August 2024

D_4	Diffuser outlet diameter
b_2	Impeller outlet width
τ	Tip clearance
Z_{gui}	Number of guide vanes
Z_{imp}	Number of impeller blades
Z_{dif}	Number of diffuser vanes
Z_{ret}	Number of return channel blades
ω_{imp}	Impeller rotation speed
ε	Total pressure ratio
η_{pol}	Polytropic efficiency
P_{t0}	Total pressure at compressor inlet
P_{t5}	Total pressure at compressor outlet
T_{t0}	Total temperature at compressor inlet
T_{t5}	Total temperature at compressor outlet
Δt	Time step
H_{n}	Normalized helicity
φ	Mass flow coefficient
Q_{m}	Mass flow rate
U_2	Impeller outlet velocity
f_{L}	Low frequency
S.S.	Suction surface
P.S.	Pressure surface
LE	Leading edge
TE	Trailing edge

1 Introduction

When the mass flow rate decreases to a specific operating point, unstable flow phenomena such as rotating stall or surge occur in the centrifugal compressor stage. These two unstable flow phenomena may reduce compressor stage efficiency, severe vibration and noise, and even shutdown, which limits the stable operation range of the centrifugal compressor stage. The flow instability mechanism has always been one of the focuses of compressor stage research. Understanding and investigating the unstable flow in the compressor stage is particularly important for developing flow control technology and broadening flow stability (Al-Busaidi and Pilidis 2016; Sun et al. 2018).

The vaned diffusers are usually assembled in centrifugal compressors to improve aerodynamic performance. However, the complex flow characteristics, such as non-uniform jet-wake flow in the circumferential direction, non-uniform flow spanwise at the impeller outlet, and strong impeller-diffuser interaction will deteriorate the flow field in the vaned diffuser (Zhao et al. 2018). For the flow instability analysis of centrifugal compressors with vaned diffusers, a lot of research work is carried out in the literature (Dawes 1995; Marsan et al. 2013; Bousquet et al. 2014; Fujisawa et al. 2016; Zamiri et al. 2017). Hunziker et al. (1994) studied the centrifugal compressor with different vaned diffusers and found that the flow characteristics of the diffuser entrance determined the flow stability inside the centrifugal compressor. Spakovszky et al. (2009) showed that bleed air near the impeller outlet could change the centrifugal compressor's spike and modal stall inception behavior. It is speculated that the unstable flow in the compressor is related to the flow in the semi-vaneless area. Joukou et al. investigated the stall inception patterns for different low-solidity cascade diffusers in a centrifugal compressor. They claimed that the rotating stall affected the diffuser semi-vaneless area's flow separation. In Skoch's study (2003), the flow characteristics inside the vaned diffuser were improved through the gas injection experiment on the semi-vaneless area at the leading edge of the vaned diffuser, increasing the surge margin. Bousquet et al. (2016) conducted a full-annulus simulation on the modal stall of the vaned diffuser. It suggested that the leading-edge vortex structures of the diffuser were the leading cause of the stall. Fujisawa et al. performed experimental measurement and numerical investigation on the diffuser rotating stall caused by vane vortex separation, which deepened the understanding of the mechanism of the rotating stall.

The research above-mentioned shows that the flow separation phenomenon may occur on the shroud/hub side of the diffuser at low mass flow rates. The flow separation will gradually develop into the diffuser rotating stall with the further decrease of mass flow rate. However, due to the limited internal space of the vaned diffuser, the installation of the measuring probes is limited. So far, there are few reports on large-scale transient measurement, which limits the full understanding of the diffuser rotating stall. Moreover, considering the possible errors in the numerical calculation under low mass flow rate conditions, high-precision experimental results are still needed to verify the numerical results, especially the instantaneous measurement results. Therefore, it is necessary to conduct multipoint and high-precision transient experimental measurements of centrifugal compressors under low mass flow rate conditions. The present study employed a high-precision measurement system for determining the instantaneous pressure fluctuation at the inlet of the vaned diffuser, and the numerical simulation is verified.

The limitation of experimental measurement is that it is difficult to effectively capture the complex flow structure in the centrifugal compressor, and the numerical calculation can make up for this shortcoming of experimental measurement. For the research on the internal flow instability of centrifugal compressors, there is a view that the URANS simulation method cannot accurately solve the turbulence scale (Hu et al. 2021), and requires a scale resolution simulation (SRS) level turbulence simulation method to solve complex flow phenomena. Meanwhile, the rotating stall changes the axial symmetry of the flow, which leads to the alternating propagation of the flow in the high and low-pressure regions (Zhao et al. 2019). The flow will appear unsteady phenomena independent of the blade passing frequency at off-design operating conditions. Therefore, to better capture the complex flow details in the centrifugal compressor under stall conditions, this paper uses detached eddy simulation (DES) and full-annulus model to study the variation of the aerodynamic performance of the compressor stage and impeller-diffuser interaction during the dynamic stall process of the vaned diffuser.

Due to conventional flow field analysis methods can only qualitatively analyze unstable flow, and advanced flow field post-processing methods (modal decomposition method) can quantitatively reveal the mechanism of unstable flow. The modal decomposition method can make up for the limitations of conventional flow field analysis methods, and further understand the instability mechanism in a turbulent flow field. Therefore, the modal decomposition method (POD and DMD) is used to analyze the flow field near the shroud side of the diffuser under stall conditions.

The present work aims to understand the stall mechanism of the vaned diffuser, the propagation law of the stall cell, the influence of the diffuser stall on the aerodynamic performance of the centrifugal compressor stage (global), as well as the impeller internal flow (local), and the unstable flow characteristics caused by the stall cells. To achieve this, experiments and full-annulus numerical simulations were conducted to investigate the flow structures at the stall operating point. The results indicate that the diffuser stall is associated with the transverse vortex formed near the shroud side of the vane suction surface. The stall disturbance caused by the stall cell exhibits a periodic propagation law at the diffuser inlet. When the diffuser stalls, there is a stall limit cycle of counterclockwise rotation between the total pressure ratio and the mass flow rate of the centrifugal compressor stage, which is closely related to the flow separation strength in the compressor stage. The modes related to the stall flow structure were analyzed using the modal decomposition method (POD and DMD). Furthermore, the flow field in the impeller and diffuser during the stall was presented to reveal the triggering mechanism and unstable flow mechanism of stall.

2 Methodology

2.1 Test Facilities Setup

This first stage of the centrifugal compressor facility was provided by Shenyang Blower Works Group Corporation. Figure 1 illustrates the structure of the test facilities. The inlet guide vanes (IGVs) are composed of 11 straight vanes that can rotate freely around its central axis, the impeller is semi-open and contains 19 backward three-dimensional blades, and the average installation angles of inlet and outlet blades are 35°and 67.5°, respectively. The vaned diffuser is composed of 20 airfoil blades, the installation angles of the inlet and outlet blades are 26.5°and 33.5°, respectively, and 18 blades in the return channel.

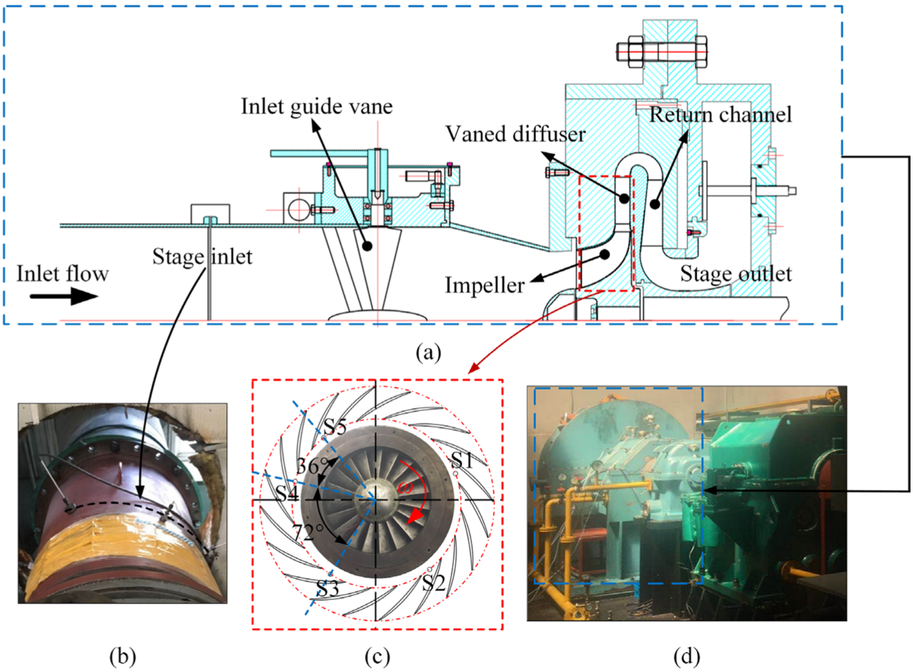

Fig. 1 Schematic of the compressor stage test rig

Table 1 Specifications of the centrifugal compressor stage (Li et al. 2021a; Zhao et al. 2016)

Parameter	Value	Parameter	Value
D_2	810 mm	Z_{gui}	11
τ/D_2	0.0042	Z_{imp}	19
b_2/D_2	0.071	Z_{dif}	20
D_3/D_2	1.11	Z_{ret}	18
D_4/D_2	1.533	ω_{imp}	5600 rpm
φ_d/Q_d (Prototype)	0.1142/16.05 kg/s	ε_b	1.55

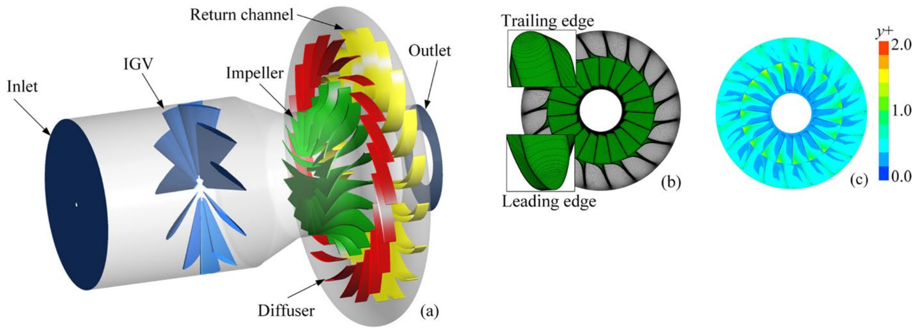

Fig. 2 Computational domain of the compressor: **a** overall domain **b** computational grid **c** y plus

The main geometric parameters of the compressor stage are summarized in Table 1. More experiment rig information can be found in the previous research (Zhao et al. 2019).

Pressure sensors are distributed non-uniformly at the diffuser entrance to examine the propagation process of rotating stall cells. The location distribution of the static pressure sensor is shown in Fig. 1c. Circumferential angles of pressure sensors S1–S2, S2–S3, and S3–S4 are 72°, while the angle between S4 and S5 is 36°. Each sensor is flush-mounted onto the inner surface of the diffuser casing to reduce the possibility of sensor interference affecting the data measurement. The dynamic probe on the sensor is the 106B52 type (PCB Piezotronics). The sampling rate was set to 20.48 kHz, and the resolution was 0.5Hz, which was considerably more significant than the shaft frequency (93.3Hz) and the blade passing frequency (BPF = 1773Hz). The sampling time was within 2 s and the acquired data was over 180 successive cycles.

2.2 Numerical Scheme

The numerical calculation of the compressor stage was carried out by using ANSYS/CFX. The full-annulus computational domain consists of the inlet pipe, IGV (inlet guide vane opening is positive 45°, based on experimental measurement), impeller, vaned diffuser, return channel, and outlet pipe are shown in Fig. 2a. The IGV upstream and the return channel downstream were extended appropriately to avoid the interference of the internal flow in the stage to the inlet and outlet boundary under stall conditions. The shear stress transport turbulence model (SST) was selected for the steady-state simulations. No-slip and adiabatic conditions were applied at solid walls. The working medium is the ideal gas (air).

The stage model (mixing plane) can obtain better flow field prediction (ANSYS, 2015). The stage model was employed as IGV-impeller, impeller-vaned diffuser, and vaned diffuser-return channel interfaces. Considering the consistency with the experimental measurement, the total pressure (98,000 Pa), and total temperature (267 K) were imposed at the stage inlet. The stage outlet boundary conditions were set to mass flow rate.

Autogrid V5 was used for structured grid division of the computational domain. To better capture the flow details in the compressor stage, especially under low mass flow conditions, the grid along all solid walls is refined. The height of the first layer grid is set to 2 μm, as shown in Fig. 2b, corresponding to y plus less than two.

Grid quality is the key to determining the accuracy of the numerical calculation results. To avoid the adverse impact of the grid quality on the numerical calculation results, five different grid numbers are used for grid independence research under the design flow condition. The results are shown in Fig. 3. The definitions of total pressure ratio and polytropic efficiency in the figure are shown in Formula 1 and 2. It is found that when the number of grids exceeds about 37.47 million, the total pressure ratio and polytropic efficiency of the compressor stage have no significant change, which can be considered grid-independent. Therefore, considering the accuracy of numerical simulation and calculation time, in the subsequent numerical calculation, the calculation model uses a grid number of about 37.47 million. The grid number of the inlet guide vane section, impeller section, blade diffuser section, and return channel section are about 9.397 million, 12.554 million, 8.448 million, and 7.071 million respectively.

$$\varepsilon = \frac{P_{t5}}{P_{t0}} \tag{1}$$

$$\eta_{pol} = \frac{\kappa - 1}{\kappa} \frac{\left(\ln \frac{P_{t5}}{P_{t0}}\right)}{\left(\ln \frac{T_{t5}}{T_{t0}}\right)} \tag{2}$$

In transient simulations, the URANS and detached-eddy simulation (DES) turbulence methods were utilized to investigate unsteady flow characteristics inside the compressor stage.

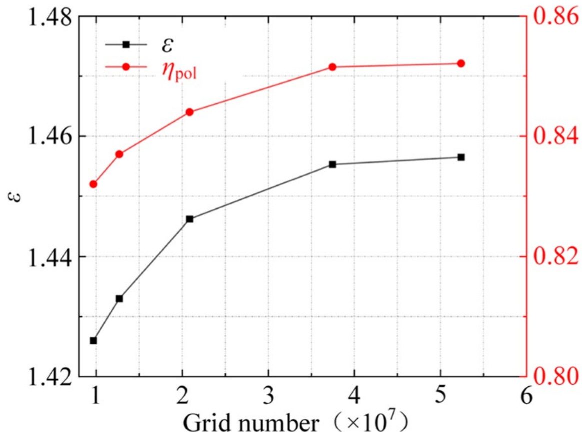

Fig. 3 Research on grid independence

The URANS simulations were employed with the SST turbulence closure model. The DES method was a hybrid scheme containing URANS (near the solid wall) and large eddy simulation (LES, flow passages) which was first applied to the study of wings by Spalart (1997). Compared with the large eddy simulation method, the detached-eddy simulation method could capture the dominant turbulence characteristics while improving the computational efficiency and has been widely used in industrial aerodynamics (Tomita et al. 2019; Broatch et al. 2016).

During transient simulations for URANS and DES, the RANS results (steady-state) were taken as the initial values of unsteady numerical calculation. To eliminate the influence of the physical time step on the transient simulation results, the size of the time step was studied. Three-time steps were chosen to calculate the static pressure at the one fixed monitoring point in the diffuser (see S1 in Fig. 1c) is shown in Fig. 4. Considering the computational accuracy and efficiency, the time step (Δt) of 2.96794×10^{-5} s (about corresponding to the impeller's rotation of one degree) was selected in this study.

2.3 Data Processing Methods for Unsteady Data

2.3.1 Vortex Identification

The vortex core identification is valuable for investigating the complicated three-dimensional flow field. The present study identified the vortex core by λ_2 vortex criteria. According to the λ_2 vortex criteria, λ_2 is the median eigenvalue of the velocity gradient tensor A ($A = S^2 + \Omega^2$, S, and Ω are symmetric and antisymmetric tensors, respectively). $\lambda_2 < 0$ represents the vortex core region identification (Jeong and Hussain 1995). The size of the vortex structure can be adjusted by setting the value of the iso-surface. Normalized helicity H_n, defined as a velocity and vorticity dot product, colored the identified vortex structure (Wu et al. 2019):

$$Hn = \frac{\vec{v} \cdot \vec{w}}{|\vec{v}| \cdot |\vec{w}|} \tag{3}$$

where $\vec{v}$ and $\vec{w}$ represent the relative flow velocity and vectors of the absolute vorticity, respectively. H_n represents the parallelism of $\vec{v}$ and $\vec{w}$. When $\vec{v}$ is parallel to $\vec{w}$, it is the

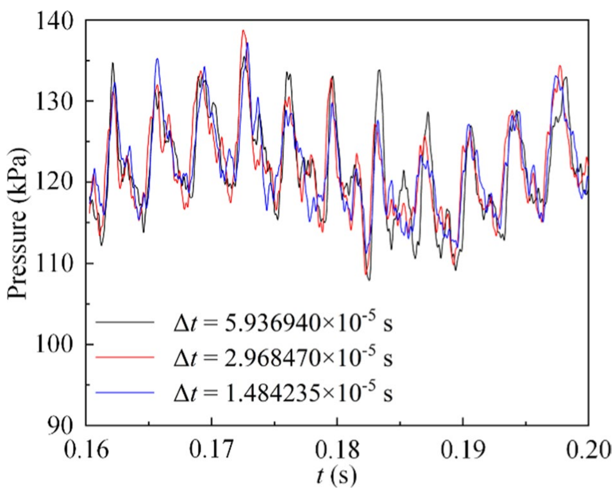

Fig. 4 Physical time step size test

position of the vortex core. Even in the case of vorticity attenuation, the vortex properties can be evaluated quantitatively (Li et al. 2020). H_n has a magnitude between -1 and 1, the sign of H_n determines the rotation direction of the vortex structure (negative magnitude means counter-clockwise rotation, and positive magnitude means clockwise rotation). Furthermore, the type of vortex structures can be classified based on their location and rotation direction, including leading-edge vortices, horseshoe vortices, tornado-like vortices, etc.

2.3.2 Modal Decomposition Methods

The POD method is used to determine the characteristics of coherent flow in the compressor stage under stall conditions. This method is utilized to determine the large-scale flow structures that cause turbulent fluctuations at different frequencies by observing the convective vortex structures' contribution to the compressor's total fluctuation energy (Wang and Liu 2017). For the fundamental of the POD algorithm, the reader is referred to Hutchinson (Hutchinson 1971) and Sirovich et al. (1987). The dominant flow structures in the centrifugal compressor can be identified by ranking the energy contribution of POD modes, and their spatial distribution and temporal evolution can be determined of the flow field by POD mode and mode coefficient, respectively (Sirovich 1987).

Due to the strong unsteady flow and multi-scale vortices characteristics in the centrifugal compressor stage, the critical flow characteristics that affect the unsteady flow are difficult to be distinguished by conventional methods. To do this, we examine the spatial–temporal characteristics of the unsteady patterns by using the data-driven DMD method (Schmid and Sesterhenn 2010). Moreover, the DMD method can provide the flow phenomenon associated with specific frequencies, which complements that the POD method cannot identify flow structures at a specific frequency. The fundamentals of the DMD method are referred to by Schmid (2010).

3 Results and Discussion

3.1 Verification of Numerical Simulation Method

To verify the rationality and accuracy of the numerical methods in this paper, the steady (RANS method) and time-averaged unsteady numerical simulation results (DES method) are compared with the experimental measurement data, as shown in Fig. 5. The abscissa in the Figure is the mass flow coefficient, which definition is shown in Formula 4, and the ordinate is the total pressure ratio and polytropic efficiency of the compressor stage, where Q_m is the mass flow rate.

$$\varphi = \frac{Q_m}{\frac{1}{4}\pi D_2^2 \rho U_2} \tag{4}$$

The numerical simulation is carried out in two steps: first, the steady calculation is used from the large flow operating point to the maximum total pressure ratio operating point, while the unsteady numerical method is used for the low flow operating points (two mass flow rates with a positive slope on the total pressure rise curve, namely OP1 ($\varphi = 0.0875$) and OP2 ($\varphi = 0.0833$)) with the unstable flow. The results (OP1 and OP2) in the figure

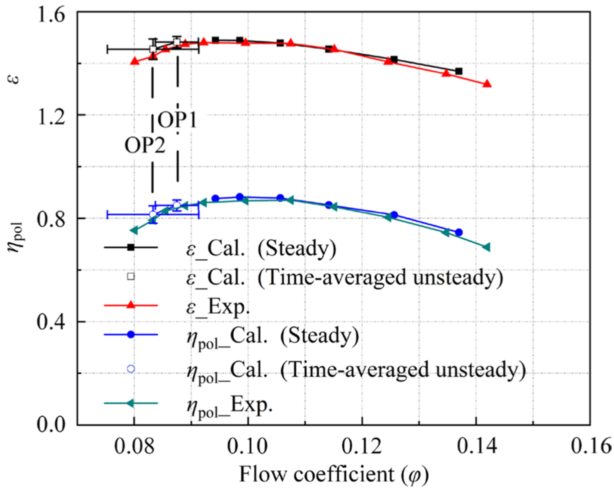

Fig. 5 Comparing of simulated results with experimental data (Zhao et al. 2019, 2016) for the compressor stage

are the time-averaged values obtained by unsteady calculation. The compressor stage's aerodynamic performance by numerical calculation was compared with the experimental measurement, as shown in Fig. 5, and the numerical results are in good agreement with the overall trend of the experimental data. According to the statistics of the difference between the numerical results and experimental data, the results show that the error between the total pressure ratio and the polytropic efficiency is less than 2%.

The comparison results of pressure fluctuation spectrum analysis at the same monitoring point are shown in Fig. 6. It can be seen from the figure that there are three discrete frequencies at the monitoring points, namely low frequency (f_L), blade passing frequency (BPF), and 2BPF at flow condition OP2, and the unstable flow in the compressor stage is mainly affected by the above three discrete frequencies. Previous studies (Li et al. 2021a) have shown that this low frequency is the stall frequency of the vaned diffuser. Moreover, it is also found that the f_L by the experimental and numerical calculation is 23.5 Hz and

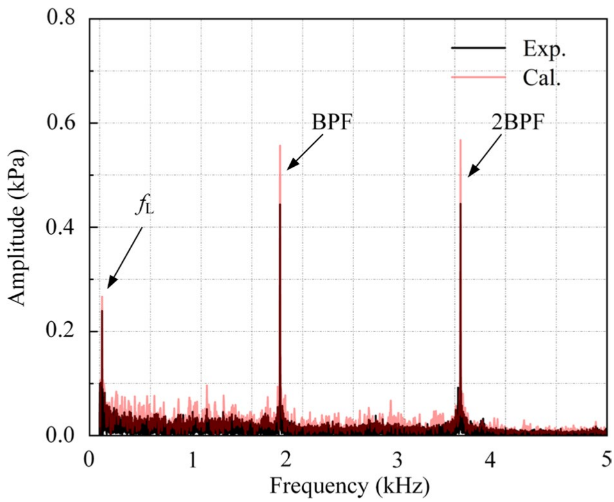

Fig. 6 Comparison of pressure fluctuation spectrum analysis of monitoring points

23.4 Hz, respectively. The main reason for this difference is due to the different frequency resolutions under the two methods. In the experimental measurement, the total sampling frequency is 20,480 Hz and the number of sampling points is 40,960, and the frequency resolution is 0.5 Hz. In the numerical calculation, the total sampling frequency is about 16,846 Hz and the number of sampling points is 5760 (16 cycles), and the frequency resolution is about 2.925 Hz. The comparison between the aerodynamic performance of Fig. 5 and the spectrum analysis of the same monitoring points in Fig. 6 shows that the numerical calculation based on the DES method can capture the same macroscopic aerodynamic performance and local unstable flow characteristics of the compressor stage as the experimental measurement. Therefore, the numerical calculation results can be used for a subsequent internal flow analysis of the compressor stage.

3.2 Influence of Turbulence Simulation Method on Numerical Results

The compressor stage's total pressure rise curve was obtained from time-averaged unsteady simulations using the DES method (Fig. 7, solid black square). DES and URANS are numerically analyzed under low mass flow rates (OP1 and OP2) to examine the influence of these methods on numerical calculations. Figure 7 compares the compressor stage's instant total pressure ratio and mass flow coefficient for the two mass flow rates. The results demonstrate that a small limit cycle appears on the left side of the maximum pressure ratio point. The limit cycle will become significantly larger as the mass flow rate decreases. However, the limit cycle size for URANS and DES turbulence methods differs. Specifically, the total pressure ratio fluctuation amplitude of the two turbulence methods for OP1 is approximately 1.54% (URANS) and 0.871% (DES) of the time-averaged value, and the mass flow rate fluctuation amplitude is approximately 7.53% (URANS) and 4.31% (DES) of time-averaged value, respectively. By decreasing the mass flow rate, the limit cycle size increases considerably. The total pressure ratio fluctuation amplitude of the two turbulence methods for OP2 is approximately 4.41% (URANS) and 2.71% (DES) of the time-averaged value, and the mass flow rate fluctuation amplitude is approximately 24.7% (URANS) and 9.64% (DES) of time-averaged value, respectively. Reducing the mass flow

Fig. 7 Comparison of compressor total pressure rise between DES and URANS methods

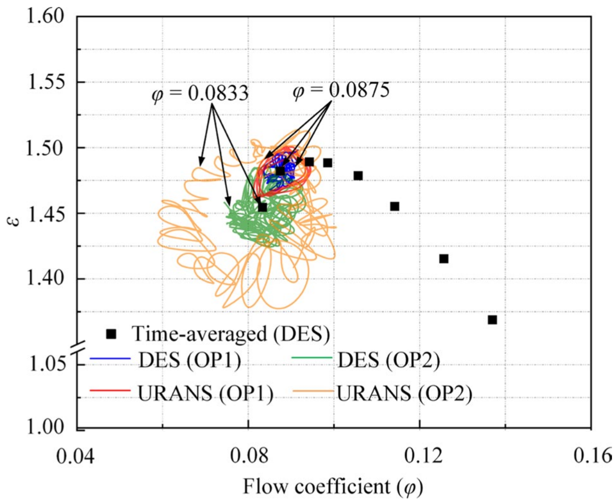

rate will exacerbate the unstable flow in the compressor stage, which is specifically manifested in the large-scale fluctuation of the compressor's aerodynamic performance.

The instantaneous results from DES and URANS methods of the leading-edge vortex (LEV) by the same threshold λ_2 value and colored by normalized helicity are shown in Fig. 8a. Due to the large positive incidence angle at the inlet of the diffuser vane's suction surface, and the strong adverse pressure gradient characteristics of the diffuser under low flow conditions, two vortex structures with opposite rotation directions are formed near the shroud side of the vane's leading-edge. The vortex structure near the suction surface rotates counterclockwise (as shown by the black dotted arrow) and impacts the suction surface of the vane, while the vortex structure away from the suction surface rotates clockwise (as shown by the black solid arrow) and develops towards the adjacent diffuser's leading-edge. The flow blockage at the inlet of the diffuser caused by the clockwise rotating vortex structure leads to the diffuser stall, which is consistent with the conclusions of the studies in the literature (Pullan et al. 2015; Bousquet et al. 2015; Everitt and Spakovszky 2013). DES method can obtain a more refined vortex structure, which shows that the DES method has a strong ability to capture the scale characteristic of the flow field, while the scale vortex structure in the URANS analysis was larger than that in the DES analysis. The main reason for this phenomenon is that the URANS method overestimates the eddy viscosity in the diffuser passages compared to the DES method and the eddy viscosity ratio in the simulation is defined as μ_t/μ (Fujisawa et al. 2014), as shown in Fig. 8b. Therefore, the DES method can more accurately predict the unsteady flow field inside the compressor stage. The flow blockage caused by the large vortex structure at the vaned diffuser's leading-edge aggravates the unstable flow in the compressor stage, which is one of the main reasons for the large limit cycle of the compressor stage in the URANS analysis.

3.3 Stall Characteristics of the Diffuser Based on Experimental Measurements

As shown in Fig. 1, the pressure fluctuation signal at the diffuser entrance was measured by experimental measurement to study the stall cell's unsteady properties. The pressure fluctuation is measured using five pressure sensors near the shroud side of the diffuser entrance, as shown in Fig. 9. The pressure changes are plotted in the rotation direction of the impeller. The pressure fluctuation traces are plotted again to form a complete revolution. The

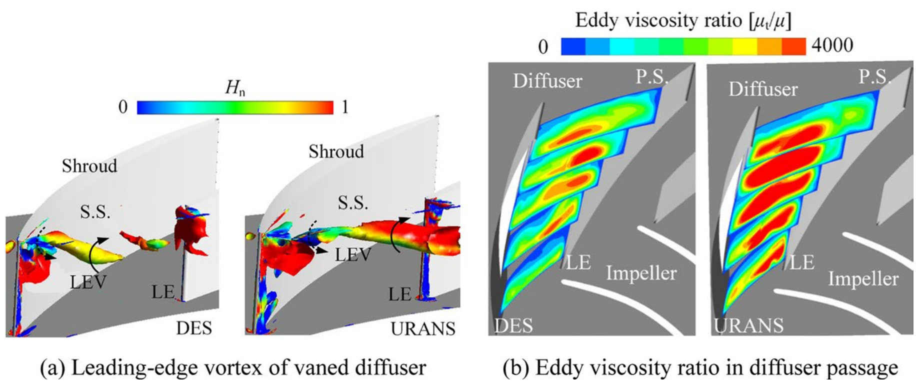

Fig. 8 Distribution of leading-edge vortex structure and eddy viscosity ratio in the vaned diffuser under different turbulence calculation methods at stall condition

black curves in the pressure fluctuation traces represent the low-pass filtered traces, and the low-pass filter frequency was set to 23.5 Hz. From the low-pass filtered traces, the disturbance caused by the stall cell propagates in the vaneless space and exhibits different patterns during the rotation of the impeller. Specifically, the stall disturbance presents periodic characteristics of arising, strengthening, decaying, disappearing, and reforming. According to the dynamic behavior of S1-S5 pressure signals, it can be evidently arbitrated that the propagation direction of the stall cell is consistent with the rotation direction of the impeller. During the propagation of the stall cell, it can be seen that the four low-pass filtered traces (S1–S4) are in the same phase at any time, but the low-pass filtered trace S5 has the inverse phase with other sensor measurement points. This reason can be explained as that according to the circumferential distribution of the sensor, the angle between S1–S2, S2–S3, and S3–S4 is 72°, while the angle between S5 and S4 is 36°, which corresponds to half of the propagation distance between the two adjacent stall cells. Moreover, the number of diffuser stall cells was found to be five, which is consistent with the conclusions of previous experiments (Zhao et al. 2019). Based on the above analysis, it was evident that this disturbance was caused by the stall cell at the diffuser entrance.

3.4 Characteristics of Stall Limit Cycle

The numerical calculation results with the DES method are used to understand the evolution of flow structures under stall disturbances in the compressor stage. Draw a curve along the maximum fluctuation extreme value of the compressor stage's total pressure ratio and mass flow rate in the limit cycle obtained under OP2 (see Fig. 7), namely the stall limit cycle, as shown in Fig. 10a. Figure 10b shows five instantaneous mass flow rates that can be used to analyze the flow field of the compressor stage under the stall limit cycle. Time A (E) and C are the maximum and minimum mass flow rate points, and time B and D are the average values in the periods of mass flow rate reduction and increase in the compressor stage. Figure 10a represents the location of the five investigated times on the stall limit cycle of the total pressure ratio of the compressor stage, and the limit cycle is counterclockwise direction, as shown by the arrow.

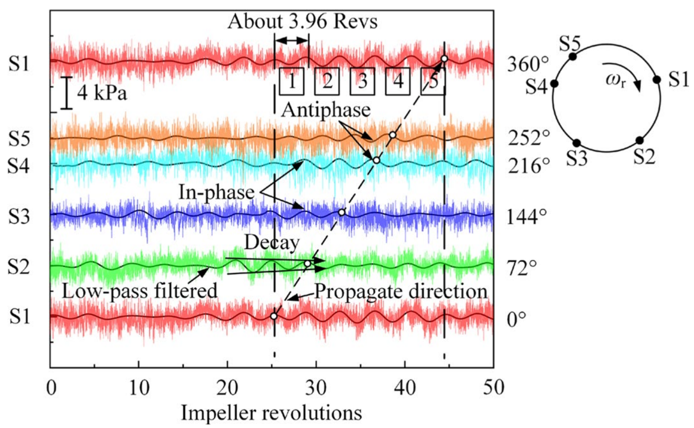

Fig. 9 Casing wall pressure fluctuation traces at diffuser entrance circumferential

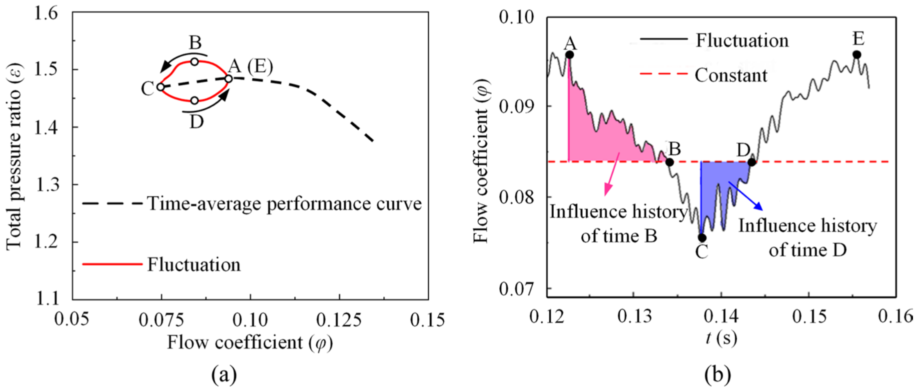

Fig. 10 Operating conditions of flow analysis (DES)

To investigate the flow characteristics in the compressor stage during the diffuser stall development, the flow structures in the impeller and diffuser at the investigated five moments were analyzed. Figure 11 demonstrates the Mach number distribution at 95% span of the diffuser at the investigated five moments. The low-momentum flow separation begins to appear at the suction side of some diffuser entrances at the time A. However, the separation vortex formed by the flow separation does not develop to the leading edge of the adjacent diffuser vanes. No apparent flow blockage was found in the diffuser passages. With the impeller's continuous rotation, the compressor stage's mass flow rate decreases gradually, and the low-velocity range on the suction side of some diffuser passages

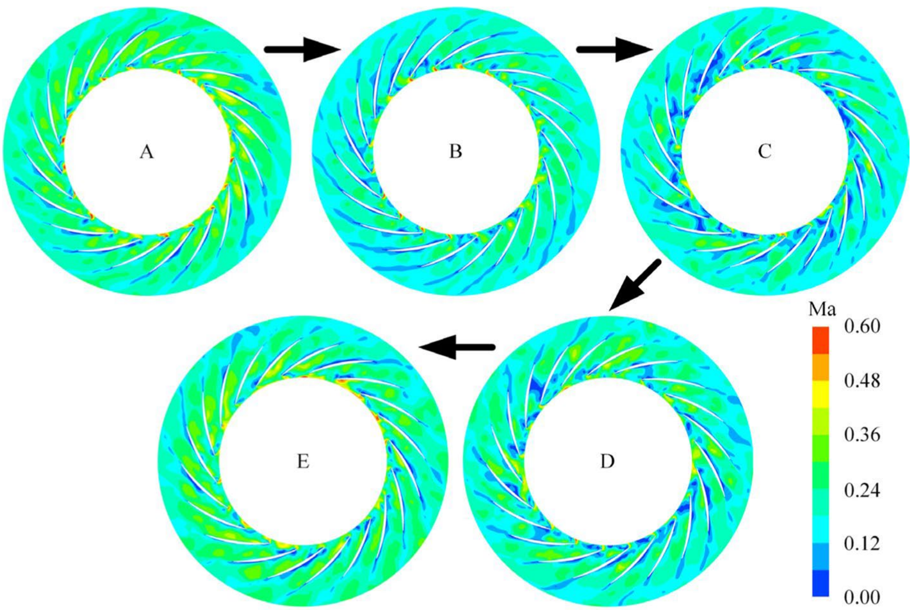

Fig. 11 Mach number distribution of diffuser 95% span during stall process

increases. At time B, the flow separation on the suction side of the vanes moves to the leading edge of adjacent diffuser vanes, realizing the circumferential propagation of stall disturbance. The diffuser passages in the compressor stage showed significant deterioration during time C of the minimum mass flow rate. The flow in the diffuser passage at time D has improved compared with time C, but the stall disturbance has continued to propagate in circumferential space. When the impeller runs to time E, the flow in all diffuser passages has been significantly improved. Similar to time A, there is no evident stall phenomenon in the diffuser passages. Therefore, the periodic fluctuation of the mass flow rate during the stall will improve the flow in the diffuser and even release the stall disturbance. However, it will retrigger a new stall disturbance under low flow conditions.

Figure 12 demonstrates the static pressure distribution at 95% span of the impeller at five moments during the diffuser stall process. The black arrow and black ellipse in the figure correspond to the position of the diffuser stall disturbance. It can be visibly seen that the flow blockage formed by the diffuser stall will affect the flow at the impeller tail, and thus form a high-pressure area (black ellipse). Moreover, a low-pressure area (red ellipse) forms at the leading edge of the impeller due to tip leakage and the suction flow, which affects the flow in the impeller and further deteriorates compressor stage performance.

Based on the above analysis, it can be concluded that there are significant differences between flow structures at times B and D with identical instantaneous mass flow rates but at different moments. Figure 13 compares the entropy increase and streamline distribution

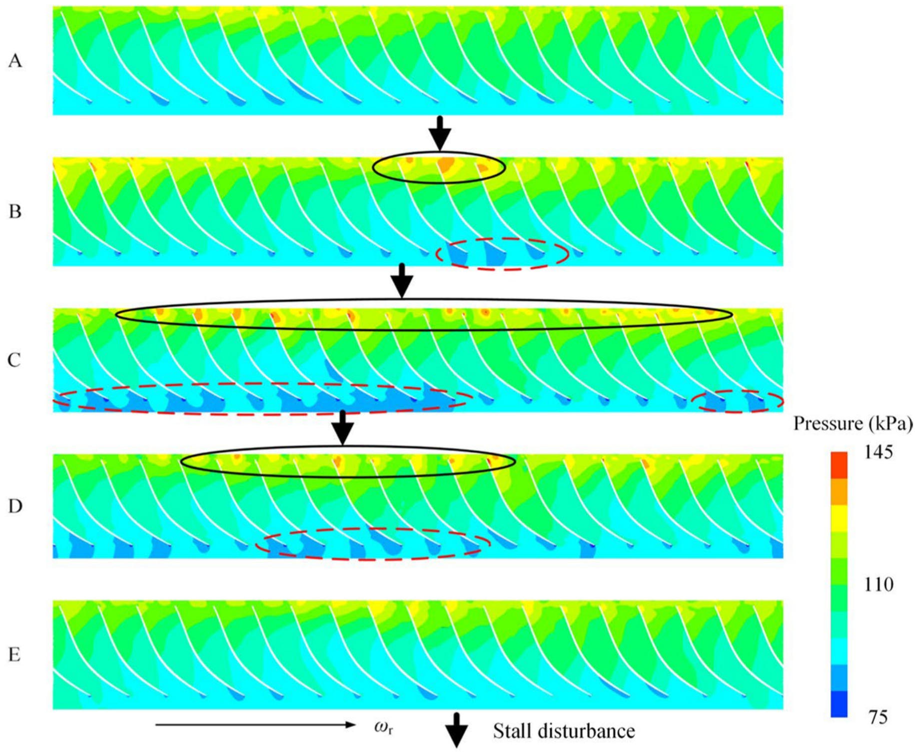

Fig. 12 Pressure distribution of impeller 95% span during stall process

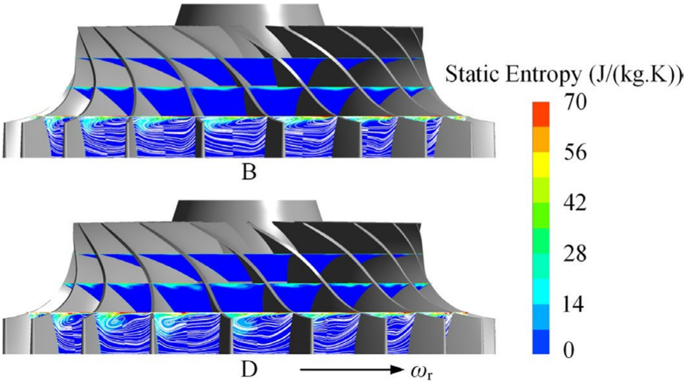

Fig. 13 Streamline and entropy increase at time B and D

Fig. 14 Schematic of velocity triangle at the impeller inlet

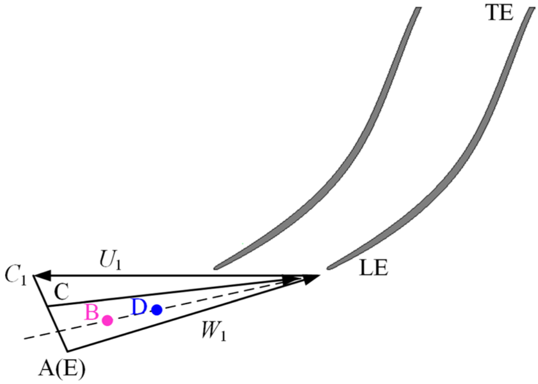

in the impeller at times B and D. The location of the secondary flow is consistent with the high entropy increase, indicating that the secondary flow is one of the leading sources of flow loss in the impeller. The entropy increase (flow loss) at time D is greater than that at time B at the three sections with different streamwise transitions, especially the average value near the impeller outlet increases by about 16.49%. From this, we can infer that the difference in the flow structure between times B and D is related to the change in mass flow rate in the stall limit cycle.

In the stall limit cycle, the stall cell in the diffuser changes the boundary conditions at the impeller outlet and then affects the flow at the impeller inlet. The velocity triangle at the impeller inlet is examined to determine how the stall limit cycle influences flow at the impeller inlet, as shown in Fig. 14. At the maximum mass flow rate (times A and E), the impeller inlet angle is close to the blade inlet angle. With the decrease in mass flow rate, the relative velocity direction becomes more tangential. The minimum relative flow angle of the impeller inlet appears at time C. Due to the mass flow rates at times B and D being identical, their instantaneous relative flow angles are the same. Nevertheless, there are significant differences between the internal flow field of the impeller at times B and D. The slope of mass flow rate at time B is $\frac{dm}{dt} < 0$, while the slope at time D is $\frac{dm}{dt} > 0$. In other words, the flow structure inside the impeller at time B changes from the previous moment.

The latter has a larger mass flow rate than time B, which is more favorable for the flow field. On the contrary, the flow field inside the impeller at time D evolves from the previous time with a lower mass flow rate, as shown in Fig. 10b. It can be inferred that the flow field and aerodynamic performance inside the impeller at times B and D are related to its influence history at the previous time. Therefore, the internal flow field of the impeller is simultaneously affected by the diffuser stall and the flow evolution history of the previous time.

3.5 Modal Decomposition Method

Two flow decomposition methods including POD and DMD methods are used to analyze the characteristics of coherent flow structure in the internal flow field of the centrifugal compressor. The dynamic process in the flow field can be represented by a POD mode (only related to space) and a POD mode coefficient (only related to time) by using the POD method. The spatial–temporal information in the unsteady flow field can be studied in more detail. The disadvantage of the POD method is that it cannot identify the flow phenomenon at a specific frequency. The DMD method can supplement this shortcoming of the POD method. Therefore, the POD and DMD methods are used to investigate the internal flow of the compressor stage under stall conditions. The resolution of the flow decomposition corresponding modal coefficient spectra is essential when investigating the rotating stall phenomenon (Semlitsch and Mihăescu 2016). Thus, the snapshot samples used in this study were consecutive time steps of 42.756 ms for 1440 instantaneous flow fields to capture the flow details in the low-frequency range. The lowest and highest frequencies captured are about 7.8 Hz and 5 kHz, respectively. Therefore, combined with the previous research (Li et al. 2021a, 2021b), it is shown that the snapshot samples chosen in this study can better capture the low-frequency phenomenon in the flow field.

To study the inducement and spatial–temporal distribution of unstable flow structures near the diffuser shroud, the POD method was used to calculate and analyze the pressure field at the 95% span of the diffuser. The results show that the first four POD modes account for about 70% of the total fluctuating energy of the pressure field at the surface, and the first to fourth POD modes account for 23.28%, 20.51%, 14.32%, and 10.92% of the total fluctuating energy of the total pressure field, respectively. When the POD mode exceeds the fourth order, the POD eigenvalues dramatically decrease, indicating that the higher-order POD modes have lower energy and a smaller overall contribution to the unstable flow field. Therefore, the spectrum analysis was conducted on the first four POD modal coefficients to reveal the domain frequency of the unstable flow field, and the amplitude is normalized by the amplitude corresponding to BPF in the first order POD mode, as shown in Fig. 15. It can be seen that the pressure fluctuation corresponding to the coherent flow structure at the near shroud side of the diffuser is mainly related to the stall frequency (f_L), BPF, and 2 BPF. The high-energy coherent flow structure in the flow field is jointly dominated by the rotating stall and the impeller-diffuser interaction in the first two order POD modes. With the increase of POD modes, the high-energy coherent flow results in the flow field are dominated by the impeller-diffuser interaction (BPF and 2 BPF).

Figure 16 shows the spatial distribution of the pressure field in the first four order POD modes corresponding to the 95% span of the diffuser. Figure 16a, b show that a large-scale flow structure appears in part of the diffuser throat, and then the diffuser passages are blocked, resulting in greater pressure fluctuations. As the order of POD modes increases, due to the weak influence of stall cells (see Fig. 15), no apparent blockage caused by large-scale flow structure is found in the diffuser throat in the third and fourth-order POD modes.

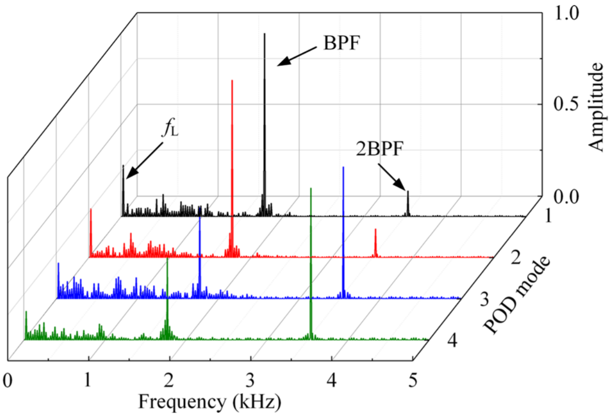

Fig. 15 The spectrum of the POD mode coefficients for the diffuser 95% span

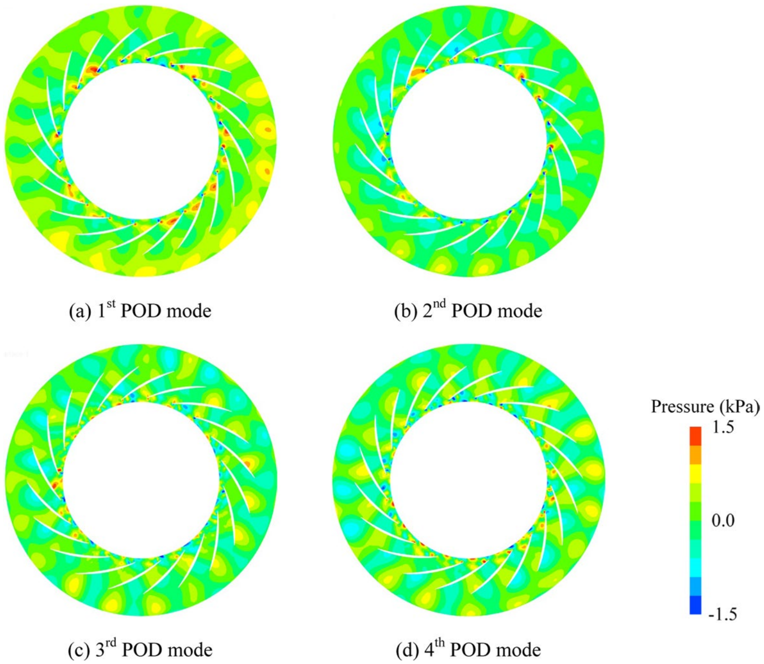

Fig. 16 The spatial distribution of the first four POD modes for the diffuser 95% span

It is worth noting that a coherent flow structure is found to propagate downstream at the diffuser outlet in the first four order POD modes, which may be related to the impeller-diffuser interaction.

As shown in Fig. 17, the diffuser surface 95% span is analyzed using the DMD for better detecting the spatial distribution of those three specific frequencies in the flow field mentioned earlier. It can be seen from Fig. 17a that the pressure fluctuation caused by the stall cell is mainly located at the diffuser throat and propagates along the circumferential direction. It can be deduced that the blockage of the diffuser throat mainly causes the diffuser

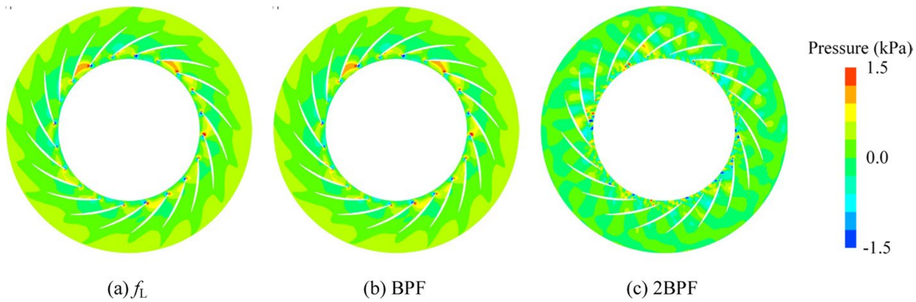

Fig. 17 The spatial distribution at specific frequency for the diffuser 95% span

stall. The pressure fluctuation caused by the impeller-diffuser interaction is more complex and propagates in the diffuser entrance, passages, and outlet (Fig. 17b, c). Although the stall cell affects the diffuser's internal flow, the diffuser's large-scale pressure fluctuation is dominated by the impeller-diffuser at this mass flow rate, which is consistent with the experimental data.

4 Conclusions

This study investigates the internal flow of the centrifugal compressor stage with a vaned diffuser under stall conditions by experimental measurement, numerical calculation, and modal decomposition method. The influence of diffuser stall disturbance on the aerodynamic performance of the compressor stage and the internal flow of the impeller and diffuser are analyzed in detail. Modal decomposition methods have been used in more detail to study the coherent flow structure in unstable flow. The main conclusions can be summarized in the following:

(1) The experimental measurement data show that it is obtained that there are five stall cells propagating circumferentially along the rotation direction of the impeller in the diffuser entrance during the diffuser stall. The stall disturbance caused by the stall cell presents a periodic propagation law of triggering, enhancing, attenuating, relieving, and retriggering at the diffuser entrance.

(2) The time-averaged unsteady numerical results obtained by the full annulus DES method show that the large positive incidence angle causes severe flow separation on the suction side of the vane diffuser entrance. Under the action of strong adverse pressure gradient and flow separation, a transverse vortex develops circumferentially near the shroud of the diffuser vane suction surface to the adjacent vane's leading-edge, this vortex blockages the diffuser passage and triggers the diffuser stall, resulting in flow instability.

(3) The unsteady calculation results obtained by the full annulus DES method shows that there is a stall limit cycle with counterclockwise rotation between the total pressure ratio and the flow rate of the stage during the diffuser stall. On the stall limit cycle, the internal flow field of the impeller is affected by the compressor stage's flow fluctuation, the diffuser stall disturbance, and the flow field in the impeller at the previous time. The entropy increase of the impeller outlet is about 16.49% at different times under the same

flow condition. Moreover, it is found that the change of the positive and negative slope region of the stall limit cycle is closely related to the strength of the flow separation in the compressor stage, that is, the severe/weak separation between the impeller and the diffuser corresponds to the positive/negative slope region of the stall limit cycle.

(4) The cause of the unstable flow in the diffuser, the dominant flow characteristics, and the unstable flow structure of the flow field under the stall frequency during the diffuser stall are revealed by the modal decomposition method. The POD results of the pressure field show that the main sources of the unstable flow in the diffuser are the stall frequency and BPF and its multiple. The BPF dominates the unstable flow inside the diffuser, indicating that the interaction between the impeller and the diffuser is the key factor for the unstable flow inside the diffuser under this flow condition. The DMD results of the pressure field show that the unstable flow area caused by the stall disturbance is mainly located at the entrance and throat of the diffuser, which leads to flow blockage in some passages of the diffuser and resulting the diffuser stall. It further reveals that the blockage of the entrance or throat of the diffuser is one of the important characteristics of the diffuser stall.

Author Contributions Yufang Zhang: Methodology, Software, Investigation, Visualization. Shuai Li: Conceptualization, Resources, Validation, Software, Writing—original draft, Writing—review & editing. Hechun Yu: Writing—review &editing, Supervision. Linlin Cui: Writing—review & editing, Data curation.

Funding This research received support from the Young Backbone Teachers Grant from the Zhongyuan University of Technology, the Key Research Project of Higher Education Institutions in Henan Province (Grant Number 24A460030), and the Key Research Project of Higher Education Institutions in Henan Province (Grant Number 22A460034).

Data Availability No datasets were generated or analysed during the current study.

Declarations

Conflict of interest The authors declare no competing interests.

References

Al-Busaidi, W., Pilidis, P.: A new method for reliable performance prediction of multi-stage industrial centrifugal compressors based on stage stacking technique: part I–existing models evaluation. Appl. Therm. Eng. **98**, 10–28 (2016)

Bousquet, Y., Carbonneau, X., Dufour, G., et al.: Analysis of the unsteady flow field in a centrifugal compressor from peak efficiency to near stall with full-annulus simulations. Int. J. Rotating Mach. **2014**, 729629 (2014)

Bousquet, Y., Binder, N., Dufour, G., et al.: Numerical simulation of stall inception mechanisms in a centrifugal compressor with vaned diffuser. J. Turbomach. **138**(12), 121005 (2016)

Bousquet, Y., Carbonneau, X., Trébinjac, I., et al.: Numerical investigation of Kelvin-Helmholtz instability in a centrifugal compressor operating near stall. ASME Paper GT2015-42495 (2015)

Broatch, A., Galindo, J., Navarro, R., et al.: Numerical and experimental analysis of automotive turbocharger compressor aeroacoustics at different operating conditions. Int. J. Heat Fluid Flow **61**, 245–255 (2016)

Dawes, W.N.: A simulation of the unsteady interaction of a centrifugal impeller with its vaned diffuser: flow analysis. J. Turbomach. **117**(2), 213–222 (1995)

Everitt, J.N., Spakovszky, Z.S.: An investigation of stall inception in centrifugal compressor vaned diffuser. J. Turbomach. **135**(1), 011025 (2013)
Fujisawa, N., Hara, S., Ohta, Y.: Unsteady behavior of leading edge vortex and diffuser stall in a centrifugal compressor with vaned diffuser. J. Therm. Sci. **25**(1), 13–21 (2016)
Fujisawa, N., Hara, S., Ohta, Y., Goto, T.: Unsteady behavior of leading edge vortex and diffuser stall inception in a centrifugal compressor with vaned diffuser. ASME paper, FEDSM2014-21242 (2014)
Fujisawa, N., Ema, D., Ohta, Y.: Unsteady behavior of diffuser stall in a centrifugal compressor with vaned diffuser. ASME Paper No.: G2017-63400
Hu, P., Lin, T., Yang, R., Zhu, X., Du, Z.: Numerical investigation on flow instabilities in low-pressure steam turbine last stage under different low-load conditions. Proc. Inst. Mech. Eng. Part a: J. Power Energy. **235**(6), 1544–1562 (2021)
Hunziker, R., Gyarmathy, G.: The operational stability of a centrifugal compressor and its dependence on the characteristics of the subcomponents. J. Turbomach. **116**(2), 250–259 (1994)
Hutchinson, P.: Stochastic tools in turbulence. Phys. Bull. **22**(3), 161 (1971)
Jeong, J., Hussain, F.: On the identification of a vortex. J. Fluid Mech. **285**, 69–94 (1995)
Joukou, S., Shinkawa, Y., Kanno, T., Kanno, T., Nishida, H., Nishioka, T., Hiradate, K.: Influence of low-solidity cascade diffuser on spike stall inception in a centrifugal compressor. ASME Paper No. GT2012-69203.
Li, R., Gao, L., Ma, C., et al.: Corner separation dynamics in a high-speed compressor cascade based on detached-eddy simulation. Aerosp. Sci. Technol. **99**, 105730 (2020)
Li, S., Liu, Y., Omidi, M., et al.: Numerical investigation of transient flow characteristics in a centrifugal compressor stage with variable inlet guide vanes at low mass flow rates. Energies **14**(23), 7906 (2021a)
Li, S., Liu, Y., Li, H., et al.: Numerical study of the improvement in stability and performance by use of a partial vaned diffuser for a centrifugal compressor stage. Appl. Sci. **11**(15), 6980 (2021b)
Marsan, A., Trébinjac, I., Coste, S., et al.: Temporal behaviour of a corner separation in a radial vaned diffuser of a centrifugal compressor operating near surge. J. Therm. Sci. **22**(6), 555–564 (2013)
Pullan, G., Young, A.M., Day, I.J., et al.: Origins and structure of spike-type rotating stall. J. Turbomach. **137**(5), 051007 (2015)
Schmid, P.J., Sesterhenn, J.: Dynamic mode decomposition of numerical and experimental data. J. Fluid Mech. **656**(10), 5–28 (2010)
Semlitsch, B., Mihăescu, M.: Flow phenomena leading to surge in a centrifugal compressor. Energy **103**, 572–587 (2016)
Sirovich, L.: Turbulence and the dynamics of coherent structures. I. Coherent structures. Q. Appl. Math. **45**(3), 561–571 (1987)
Skoch, G.J.: Experimental investigation of centrifugal compressor stabilization techniques. J. Turbomach. **125**(4), 704–713 (2003)
Spakovszky, Z.S., Roduner, C.H.: Spike and modal stall inception in an advanced turbocharger centrifugal compressor. J. Turbomach. **131**(3), 031012 (2009)
Spalart, P.R.: Comments on the feasibility of LES for wings, and on a hybrid RANS/LES approach. In: Proceedings of First AFOSR International Conference on DNS/LES. Greyden Press (1997)
Sun, Z., Zheng, X., Kawakubo, T.: Experimental investigation of instability inducement and mechanism of centrifugal compressors with vaned diffuser. Appl. Therm. Eng. **133**, 464–471 (2018)
Tomita, I., Ibaraki, S., Wakashima, K., et al.: Effects of flow path height of impeller exit and diffuser on flow fields in a transonic centrifugal compressor. ASME Paper GT2015-43271 (2019)
Wang, P., Liu, Y.: Unsteady flow behavior of a steam turbine control valve in the choked condition: Field measurement, detached eddy simulation and acoustic modal analysis. Appl. Therm. Eng. **117**, 725–739 (2017)
Wu, Y., An, G., Chen, Z., et al.: Computational analysis of vortices near casing in a transonic axial compressor rotor. Proc. Inst. Mech. Eng. Part g: J. Aerosp. Eng. **233**(2), 710–724 (2019)
Zamiri, A., Lee, B.J., Chung, J.T.: Numerical evaluation of transient flow characteristics in a transonic centrifugal compressor with vaned diffuser. Aerosp. Sci. Technol. **70**, 244–256 (2017)
Zhao, P.F., Liu, Y., Li, H.K., et al.: The effect of impeller–diffuser interactions on diffuser performance in a centrifugal compressor. Eng. Appl. Comput. Fluid Mech. **10**(1), 565–577 (2016)
Zhao, J., Wang, Z., Zhao, Y., et al.: Investigation of transient flow characteristics inside a centrifugal compressor for design and off-design conditions. Proc. Inst. Mech. Eng. Part a: J. Power Energy **232**(4), 364–385 (2018)
Zhao, X., Zhou, Q., Yang, S., et al.: Rotating stall induced non-synchronous blade vibration analysis for an unshrouded industrial centrifugal compressor. Sensors (basel, Switzerland) **19**(22), 4995 (2019)

Publisher's Note Springer Nature remains neutral with regard to jurisdictional claims in published maps and institutional affiliations.